A 3D-transient elastohydrodymanic lubrication hip implant model to compare ultra high molecular weight polyethylene with more compliant polycarbonate polyurethane acetabular cups.

Audrey Ford[a], Zikai Hua[b], Stephen J. Ferguson[c], Lisa A. Pruitt[a], Leiming Gao[d]

[a] *Department of Mechanical Engineering, 6141 Etcheverry Hall, Mail Code 1740, University of California Berkeley, Berkeley, CA 94720-1740, USA*
[b] *School of Mechatronics Engineering and Automation, Shanghai University, 266 Jufengyuan Rd, Baoshan, Shanghai, China*
[c] *Institute for Biomechanics, ETH Zurich, Leopold-Ruzicka-Weg 4, 8093 Zurich, Switzerland*
[d] *Engineering Department, School of Science and Technology, Nottingham Trent University, 50 Shakespeare Street, Nottingham, NG1 4FG, United Kingdom*

Abstract

Wear remains a significant challenge in the design of orthopedic implants such as total hip replacements. Early elastohydrodynamic lubrication modeling has predicted thicker lubrication films and, consequently, improved friction and wear performance in compliant polycarbonate polyurethane (PCU) bearing materials compared to stiffer materials like ultra-high molecular weight polyethylene (UHMWPE). However, experimental wear studies showed mixed results compared to the model predictions. The mismatch between model and experimental results may lie in the simplifying assumptions of the early models such as: steady state, one dimensional rotation and loading, and high viscosities. This study applies a 3D-transient elastohydrodymanic model based

Email address: `leiming.gao@ntu.ac.uk` (Leiming Gao)

on an ISO standard gait cycle to better understand the interaction between material stiffness and film thickness in total hip arthroplasty material couples. Similar to previous, simplified models, we show that the average and central film thickness of PCU (~ 0.4 μm) is higher than that of UHMWPE (~ 0.2 μm). However, in the 3D-transient model, the film thickness distribution was largely asymmetric and the minimum film thickness occurred outside of the central axis. Consequently, although the overall film thickness of PCU was higher than that of UHMWPE, the minimum film thickness of PCU was lower than that of UHMPWE for the majority of the gait cycle. The minimum film thickness of PCU also had a larger range throughout the gait cycle. Both materials were found be be operating between boundary and mixed lubrication regimes. This 3D-transient model reveals a more nuanced interaction between bearing material stiffness and film thickness that supports the mixed results found in experimental wear studies of PCU hip implant designs.

Keywords: Elastohydrodynamic Lubrication, orthopedic biomaterials, hip arthroplasty, polycarbonate polyurethane, ultra high molecular weight polyethlyene

---

1. Introduction

The demand for total hip replacements is predicted to increase driven by a greater number of younger patients placing increasing demands on the performance and lifespan of the device Kurtz et al. (2009); Kurtz (2015). Currently, wear is the major failure mode limiting the life of total hip replacements with a polymer (largely ultra-high molecular weight polyethylene (UHMWPE)) bearing surface articulating against a metal or ceramic femoral head Sonntag et al. (2012); Smith and Hallab (2009); Willert et al. (1990); Goodman et al. (2006); Jacobs et al. (2006); Atwood et al. (2011). Consequently, wear has been targeted in the effort to design longer-lasting, higher-performing total joint replacements to meet the increasing demand.

One proposed solution to improve wear performance is to replace UHMWPE with a more compliant bearing material Sonntag et al. (2012). A softer material allows greater deformation. Increased deformation increases the contact area, consequently reducing contact stresses. Further, the softer materials promote better lubrication regimes to reduce friction Flannery et al. (2010); Scholes et al. (2007); Kanca et al. (2018); Auger et al. (1995). These hypotheses were supported by elastohydrodynamic lubrication (EHL) modeling that solved the coupled fluid dynamics of the synovial fluid with elastic deformation of the contacting acetabular cup and femoral head Dowson and Jin (1986); Jin and Dowson (2005); Wang and Jin (2006); Jin et al. (1993); Mattei et al. (2011). EHL modeling has been experimentally validated by optical interferometry Jin et al. (1994).

Initial parametric EHL studies showed an increase in lubricant thickness and reduced fluid pressure with lower modulus of the acetabular cup Dowson et al. (1991); Wang et al. (2004). Additionally, the lubricant thickness predicted by Dowson et al. (1991); Wang et al. (2004) was thicker or on the order of the reported surface roughnesses Elsner et al. (2011); Scholes et al. (2006), suggesting a full-fluid film lubrication regime, ideal for minimizing wear.

The predicted lubrication regimes with compliant materials supported the use of alternate polymers with a lower modulus in total joint replacement, such as polycarbonate polyurethane (PCU) copolymers. PCU can be produced with a modulus ranging from 11 - 1000 MPa compared to the 700 - 1000 MPa modulus of UHMWPE Ghaill and Little (2008); Kanca (2017); Ford et al. (2018); Kurtz et al. (1998); Malito et al. (2018); Kurtz (2015) used in previous EHL studies Jalali-Vahid et al. (2001); Jalali-Vahid and Jin (2002); Jalali-Vahid et al. (2003); Wang et al. (2004). Additionally, PCU is highly elastomeric with a high energetic toughness making it an attractive candidate for long-term load bearing. PCU has been commercialized as an acetabular cup bearing material in the Tribofit® device by Active Implants (Memphis, TN, USA) Sonntag et al. (2012); Siebert et al. (2008); Wippermann et al. (2008); Ianuzzi et al. (2010). Experimental wear studies and clinical results provide insight into the the wear performance of PCU acetabular cups compared to the EHL model predictions.

Experimental studies tested the wear performance of polyurethane bearing surfaces for the validity of the modeling results. Some studies showed positive results with respect to friction and wear performance compared to conventional UHMWPE Elsner et al. (2010, 2011); St. John and Gupta (2012). The overall wear rate of PCU implants (5 - 19 mm^3/million cycles) Elsner et al. (2010, 2011); St. John and Gupta (2012) is lower than the wear rate of conventional UHMPWE (17.1 - 56.7 mm^3/million cycles) St. John and Gupta (2012); Sonntag et al. (2012). However, the wear rate of PCU was similar to or higher than the wear rates reported for highly-crosslinked UHMWPE (4.7 - 8.1 mm^3/million cycles) Sonntag et al. (2012). PCU wear rates similar to the experimental results have been reported in limited explant studies (13 - 15 mm^3/million cycles) Siebert et al. (2008); Wippermann et al. (2008).

Beyond the total wear rate, the PCU wear particles created in simulator studies were larger (8 - 13 μm) than those reported for UHMPWE (0.1 - 5 μm). Larger particles have been correlated to potentially leading to less inflammatory immune response Elsner et al. (2010, 2011); Smith and Hallab (2009). In contrast, an explant study of PCU implants reported smaller average wear particle size than that reported in the simulator studies (0.9 - 2.9 μm) Wippermann et al. (2008).

Clinical results of the outcomes of implants with PCU acetabular cups are also mixed, reporting positive results, but also citing wear-related revisions Giannini et al. (2011); Moroni et al. (2011); Cadossi et al. (2013). The mixed results of experimental wear studies and limited clinical data do not corroborate the EHL models that predicted better lubrication regimes.

The simplifying assumptions of the early EHL models are a possible explanation for the misalignment between the computational and experimental results. The early EHL modeling assumed 1D flexion-extension loading and steady-state rotation conditions Dowson et al. (1991); Wang et al. (2004).

In some studies, a non-physiologically high value for viscosity of the synovial fluid (0.01 Pa·s) was used to promote stability of the solution Dowson et al. (1991); Jin et al. (1994). Recently, large advancements have been made to the EHL model of hip replacements Mattei et al. (2011); Gao et al. (2009, 2018); Lu et al. (2018). Work by Gao et al. published a solution for 3D transient solution for metal on metal hip replacements Gao et al. (2009). Other models have been developed to incorporate the viscoelastic mechanical response of UHMWPE and to incorporate wear into a transient solution Lu et al. (2018); Putignano and Dini (2017); Gao et al. (2018).

The objective of this study was to compare the the lubrication regimes in hip replacement with a PCU and UHMWPE bearing surface using a 3D-transient gait loading pattern based on the ISO 14242 standard. We hypothesize that the assumptions of 1D rotation and loading and steady-state conditions used in previous compliant bearing surface models led to an over-prediction of the lubrication regimes. Using a 3D-transient gait loading pattern, we aim to better simulate the experimental performance of the implant. A more physiologically accurate model description will provide a better understanding of the lubrication regimes and their contribution to wear mechanisms in order to design longer lasting hip implants.

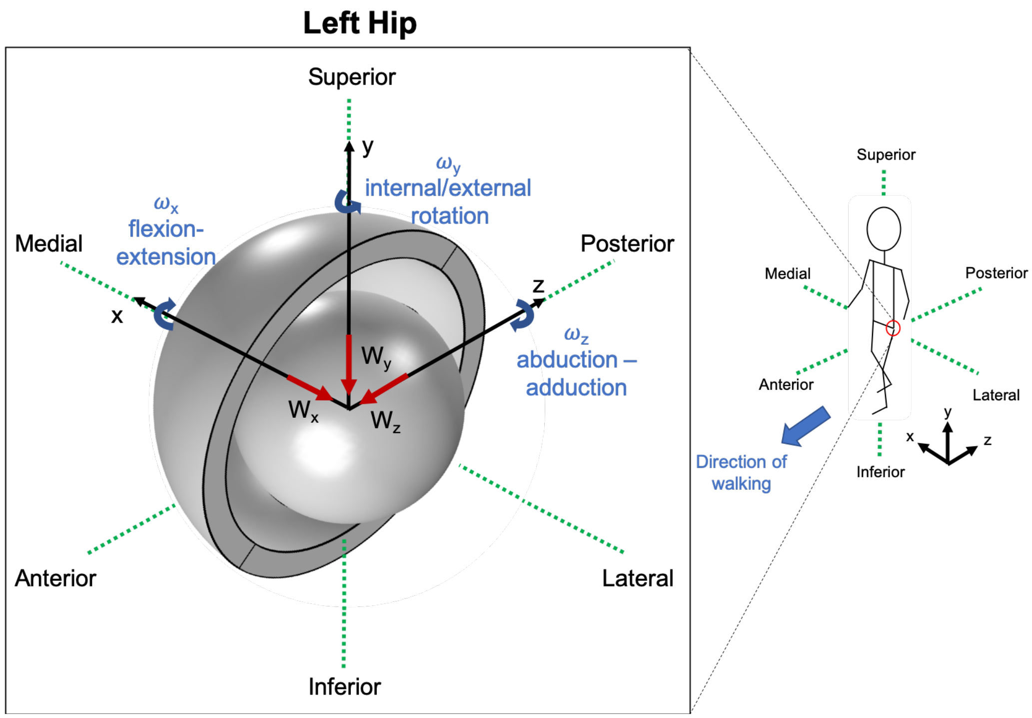

Figure 1: We modeled a left hip implant with an external loading based on the walking gait cycle and the coordinate system shown here.

2. Methods

2.1. Geometry and materials

This study compared a compliant bearing material, PCU, to the current clinical standard, UHMWPE (Figure 1). The geometry of the PCU device was based on the smallest clinical available geometry (34 mm diameter, 3 mm thickness). The small diameter was selected because previous EHL studies have shown that the smaller cup diameters have lower film thicknesses and therefore represent the most challenging design Wang et al. (2004). A UHMWPE cup of identical geometry was also modeled. Clinically, UHMWPE acetabular cups tend to have smaller diameters to increase the cup thickness to accommodate known wear challenges. This geometry is also what has been previously modeled using EHL. In order to compare with previously published results, as a control, we also modeled a UHMWPE acetabular cup with a smaller diameter (28 mm). The modulus of the smaller diameter UHMWPE cup was also reduced to validate our model against previously published work Lu et al. (2018). The radial clearance modeled was 50 μm, in line with previous studies Lu et al. (2018); Mattei et al. (2011). The geometries and material properties that were modeled are summarized in Table 1.

Table 1: Summary of geometry and material properties used in each test case.

	Case 1	Case 2	Case 3
Material	PCU	UHMWPE	UHMWPE
Radius (r, mm)	17	17	14
Cup thickness (t, mm)	3	3	7
Clearance (c, μm)	50		
Viscosity (η, Pa·s)	0.01 & 0.002		
Elastic Modulus (E, MPa)	24	1000	700
Poisson's Ratio (ν)	0.4924	0.4	0.4

Two loading scenarios were modeled for each test case: steady state and transient. The steady state solution in 1D applied a flexion-extension angular velocity of 2 rad/s with a vertical load of 1500 N. The transient solution utilized ISO 14242 loading parameters to mimic the 3D loads and velocities of a physiological gait cycle (Figure 2). The total cycle was discretized into 100 time steps.

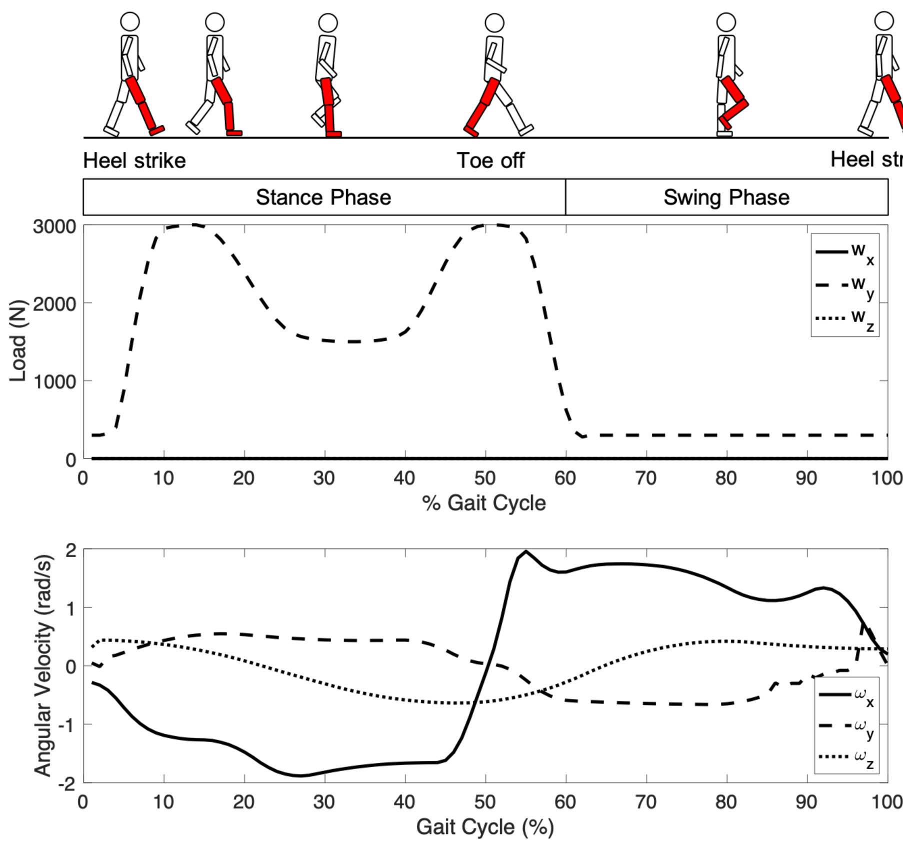

Figure 2: The ISO 14242 simulated gait cycle was used as the loading input for the model. The 3D loading and rotations were used as inputs at 100 discrete time points to simulate a single walking gait cycle.

2.2. EHL Solution

The EHL model couples both the thin-film fluid flow and the deformation of the structure, implemented in three steps. First, given the load and rotation inputs from the ISO gait cycle and an assumed initial gap, the Reynolds equation for the fluid pressure distribution was solved. Second, the elastic deformation of the acetabular cup resulting from this pressure distribution was calculated. Third, the elastic deformation was used to adjust the initial gap and update the fluid thickness (Figure 3). Thereafter, the problem was iteratively solved until the convergence criteria of load balance and fluid pressure was met. This iterative process was repeated discretely at all time points in the gait cycle until a converged cycle was reached, giving the final solution.

The model utilized the solution for the Reynold's equation in spherical coordinates (Equation 1).

$$\begin{aligned}\frac{\partial}{\partial\phi}\left(h^3\frac{\partial p}{\partial\phi}\right)+sin\theta\frac{\partial}{\partial\theta}\left(h^3 sin\theta\frac{\partial p}{\partial\theta}\right)=6\eta R_c^2 sin\theta\Bigg[&-\omega_x\left(sin\phi sin\theta\frac{\partial h}{\partial\theta}+cos\phi cos\theta\frac{\partial h}{\partial\phi}\right)\\&+\omega_y\left(cos\phi sin\theta\frac{\partial h}{\partial\theta}-sin\phi cos\theta\frac{\partial h}{\partial\phi}\right)\\&+\omega_z sin\theta\frac{\partial h}{\partial\phi}\Bigg]\\&+12\eta R_c^2 sin^2\theta\frac{\partial h}{\partial t}\cdot dyn\end{aligned}\tag{1}$$

where h is the fluid thickness, p is the fluid pressure, η is the fluid viscosity, R_c is the cup inner radius, ω is the rotational velocity in x, y, and z directions in the global coordinate system of the applied load, and dyn is a

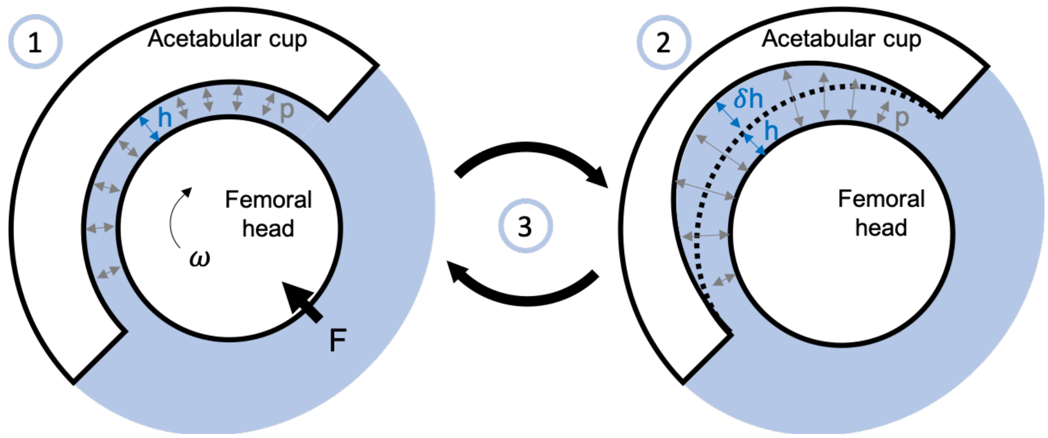

Figure 3: The EHL solution is an iterative process to solve for the film thickness and pressure distribution in lubricated contact. First, a film thickness (h) is assumed and, by solving the Reynolds equation, a pressure obtained that is in equilibrium with the applied loads (F, ω). Second, the pressure is used to determine the resulting deformation of the acetabular cup (δh). The film thickness is adjusted to include the deformation ($h+\delta h$) and the first step is repeated to obtain a new pressure distribution. This process is iteratively repeated until a converged solution is obtained.

switch parameter between the transient and steady state conditions. A zero pressure boundary condition was used to ensure that pressures were positive or zero everywhere.

No anatomical angle (β) was applied to the cup as this has been shown to have little impact on the solution Mattei et al. (2011). The transformation between the global reference frame of the ISO standard gait loading (x, y, z) and the spherical cup mesh of the Reynold's solution (θ, ϕ, Figure 4) was given as

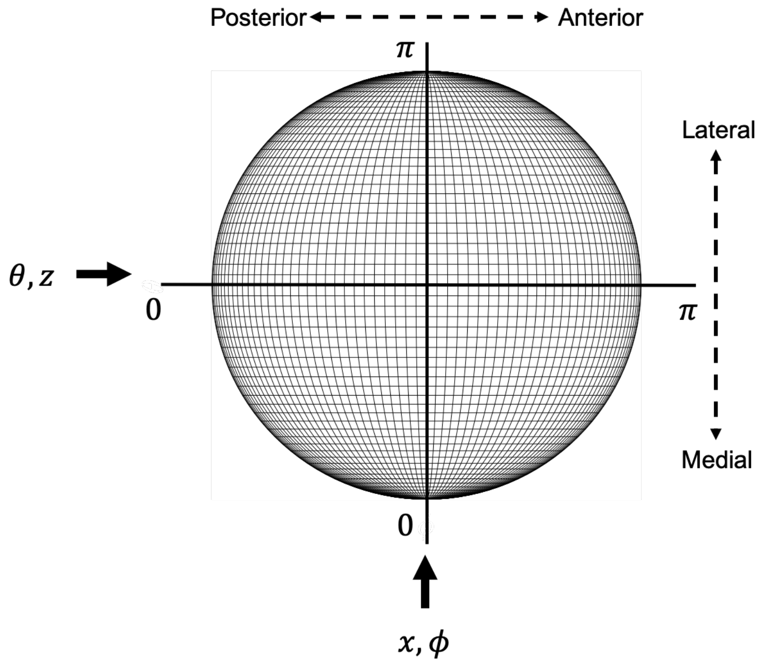

Figure 4: The acetabular cup was meshed with a spherical mesh in ϕ and θ from 0 to π. The z and x axes are labeled to show the relationship to the external loading coordinates from Figure 1.

$$\begin{aligned} p_x &= psin^2\theta cos\phi \\ p_y &= psin^2\theta sin\phi \\ p_z &= psin\theta cos\theta \end{aligned} \tag{2}$$

To maintain equilibrium, the resulting pressure distribution from the Reynold's equation must be equivalent to the applied load from the gait cycle.

$$f_{x,y,z} = R_c^2 \int_\phi \int_\theta p_{x,y,z} d\theta d\phi = -w_{x,y,z} \tag{3}$$

Within the Reynold's equation, the fluid thickness was defined as a function of the radial clearance, eccentricities between the acetabular cup and femoral head in x, y, and z directions, and the elastic deformation of the acetabular cup under the fluid pressure.

$$h(\phi,\theta) = c - e_x sin\theta cos\phi - e_y sin\theta sin\phi - e_z cos\theta + \delta(\phi,\theta) \tag{4}$$

2.3. Elastic deformation

The elastic deformation of the acetabular cup was estimated by linearly mapping displacements as a function of the distance from a point of loading.

$$\delta = f(\Delta s) \tag{5}$$

where δ is the displacement and Δs is the spherical distance between point of displacement and the point of loading. The solid model of the acetabular cup incorporating the linear elastic material properties and geometry of test cases was created in COMSOL Multiphysics (Stockholm, Sweden). The spherical mesh identical to that used in the EHL model was generated. The outside surface of the cup component was constrained in all degrees of freedom. Pressure loading was applied on the inside surface of the cup. All materials were modeled as linear elastic.

In the methodology there are two assumptions;

Assumption 1. Linear material property. The finite element model in COMSOL was established based on this assumption.

Assumption 2. Displacements as a discrete function of spherical distance are independent to the location on the surface, i.e. the dependent variable in Equation 5 is only δs, ϕ or θ are not included. The deformation calculation was based on this assumption. An influence coefficient matrix $\mathbf{K}$ with reduced order of $n\ x\ n$ was used instead of the full size matrix of $n^2\ x\ n^2$. This allows the implementation of the Multi-level Multi-integration or FFT method in EHL to quickly calculate the integral in Equation 6.

$$\delta(\phi,\theta) = \int_{\phi}\int_{\theta} K(\phi-\phi',\theta-\theta')\cdot p(\phi',\theta')d\theta d\phi \tag{6}$$

The basic mapping method was the same as described in previous EHL models of hip implants. However, the method was significantly improved in terms of collecting the relevant data for mapping, resulting in reduced time cost and numerical complexity. The data of displacements used to map the function 7 were obtained from only one finite element calculation, with a unit pressure applied to one element at the centre of the cup ($\phi = \theta = 90°$), as shown in Figure 5. It was validated by comparing the displacements due to other non-central loadings ($\phi = 30° \sim 90°, \theta = 90°$) as shown in Figure 6, and the comparison errors were less than 5%. When the loading point was very close to the edge the errors could increase significantly, however under normal gait conditions the contact location was generally $> 30°$ away from the edge of the cup.

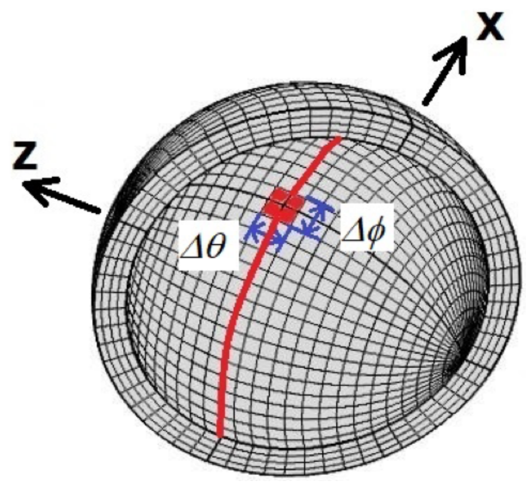

Figure 5: The linear mapping of displacements was based on a unit pressure that was applied to the central node ($\delta\phi\ x\ \delta\theta$).

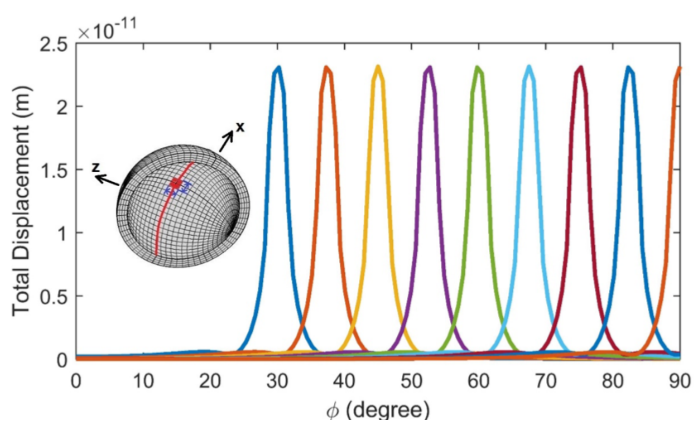

Figure 6: The error in the displacements, calculated at different locations on the cup, was shown to be less than 5% between $\phi = 30° \sim 90°, \theta = 90°$.

Once the mapped function was obtained it was used to generate the order-reducted influence coefficient matrix ($\mathbf{K}$) with the size of $n\ x\ n$. In each ϕ

and θ direction the number of nodes is n. Assuming rotational symmetry in both the ϕ and θ directions, the full matrix had a dimension of n^2 x n^2 with the element values representing the displacement of all nodes as a function of distance to the loaded node. To validate the performance of the influence coefficient matrix ($\mathbf{K}$), the deformation calculated by the current method (Equation 8) was compared to the finite element result from COMSOL. Several pressure distributions, as described in Equation 7, were used in the validation. The pressure distributions roughly represented the maximum pressure (10 MPa) distribution of the gait cycle. The normal deformations along the central cross-section of the cup surface are shown in Figure 7 and the errors are listed in Table 2.

$$\begin{aligned} p &= p_0 \cdot max\left[1 - 2\left(\frac{x}{R}\right)^2 - 2\left(\frac{z}{R}\right)^2, 0\right] \\ p_0 &= 10^7 Pa \end{aligned} \tag{7}$$

$$\begin{aligned} \delta(i,j) = \sum_{k,l=0}^{n} K(|i-k|, |j-l|) \times P(k,l) \\ i,j,k,l = 0,...,n \end{aligned} \tag{8}$$

The governing equations were non-dimensionalized and discretized as has been previously described Gao et al. (2009, 2018). Multigrid methods were used to accelerate convergence. Three grid levels were used: 64 x 64, 128 x 128, and 256 x 256. The convergence criteria were based on the error in the pressure and angular velocities in x, y, and z. The convergence criteria are listed in Table 3.

Table 2: The errors in deformation calculated by the mapped **K** matrix compared to the FE model.

Mesh grid	Error (%) PCU (E = 24 MPa)	UHMWPE (E = 700 MPa)	UHMWPE (E = 1 GPa)
n = 64	0.69	0.29	0.62
n = 128	0.3	0.22	0.12
n = 256	0.26	0.22	0.033

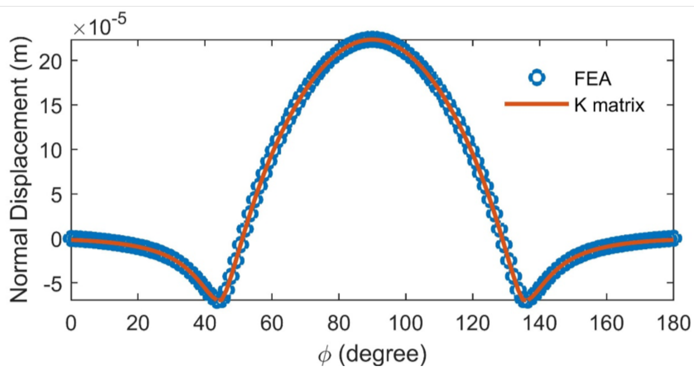

Figure 7: The deformations along the central cross-section of the PCU cup surface were calculated using a finite element model and the **K** matrix from the pressure given in Eq. 7 on mesh grid $n = 256$ and compared.

2.4. Lubrication regimes

The comparison of the film thickness is important because of its influence on the wear potential of the surface couple through the hydrodynamic lubrication regime. Lubrication regimes (λ) are defined as the ratio of the minimum film thickness (h_{min}) to the average surface roughness (R_a) of the material couple:

Table 3: Convergence criteria used in solutions.

Error	Convergence Criteria
w_x	0.01
w_y	0.005
w_z	0.01
p	0.005

$$\lambda = \frac{h_{min}}{R_a} \tag{9}$$

where boundary lubrication regime (highest wear potential): $0.1 \leq \lambda < 1$, mixed lubrication regime (middle wear potential): $1 \leq \lambda < 3$, and full fluid film lubrication regime: $\lambda \geq 3$. The average surface roughness of the material couple was approximated as the roughness of the polymer which is assumed to be greater than that of the metal or ceramic femoral head Mattei et al. (2011).

3. Results

The solution for the steady state case with an average applied load of 1500 N was used to validate the model against previously published results. Our model predicted a central film thickness of 0.19 μm for an UHMWPE acetabular cup (η=0.002 Pa·s, E = 1 GPa, R = 17 mm) while a similar model by Wang et al predicted an average film thickness of 0.11 μm (η = 0.0025 Pa·s, E = 1 GPa, R = 14 mm) Wang et al. (2004). For a PCU acetabular cup, our model predicted a central film thickness of 0.88 μm (η = 0.002 Pa·s, E = 20 MPa, R = 17 mm) while a similar model by Wang et al predicted an average film thickness of 0.17 μm (η = 0.002 Pa·s, E = 20 MPa, R = 16 mm) and 0.36 μm (R = 23 mm) μm Wang et al. (2004). Although differences in model parameters and the reporting of average versus central film thicknesses make it difficult to directly compare the models, the values and trends observed are similar.

Similar to what has been previously reported Wang et al. (2004), our results show that the central and minimum film thickness of PCU was greater than that of UHMWPE for both the identical geometry (r = 17 mm), and a smaller diameter geometry for UHMWPE (r = 14 mm) (Figure 8).

Figure steady state pcu vs UHMPE film thickness

The transient solution for the UHMWPE couple control (28 mm diameter, E = 700 MPa, η = 0.01 Pa·s) was similar to that reported by Liu et al, with a fluid pressure varying between 2 and 10 MPa and a minimum film thickness of around 0.5 μm. Lu et al. reported a larger variation in the film thickness throughout the gait cycle.

Similar to the steady state solution, the transient solution predicts a higher film thickness along a central transect for the PCU couple (0.13 - 0.24 μm) compared to a UHMWPE couple (0.05 - 0.16 μm) with identical

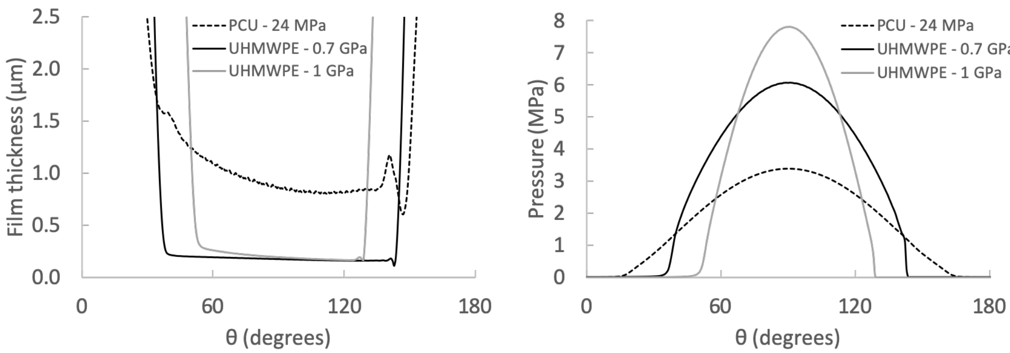

Figure 8: Similar to previously reported steady state results, the film thickness of PCU was higher than that of UHMWPE acetabular cups. The opposite is true of the pressure, which is lower for PCU than for UHMWPE (Elastic modulus indicated in legend, $\eta = 0.002 Pa \cdot s$, F = 1500 N).

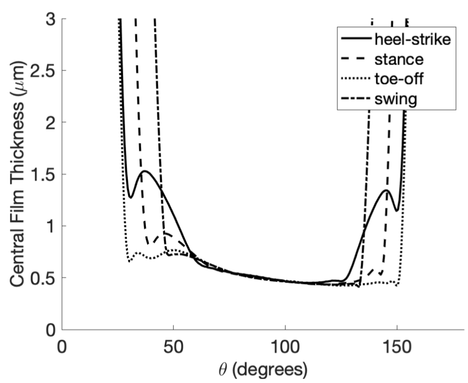

Figure 9: The transient solution of an UHMWPE acetabular cup (radius = 14 mm, elastic modulus = 700 MPa, $\eta = 0.01 Pa \cdot s$) was used as a reference to compare to previously published work Lu et al. (2018). Our solution agreed well with the predicted minimum film thickness by Liu et al. of approximately 0.5 μm.

geometry (Figure 10 & 11). The film thickness profile of PCU in the entraining direction varies more across the contact area than that of UHMWPE. For UHMWPE, there is less difference between the leading and lagging film thickness than between the leading and lagging film thickness of the PCU couple. For both UHMWPE and PCU, the impact of the varying load and motion throughout the gait cycles has a more pronounced impact on the contact area rather than the minimum film thickness profile.

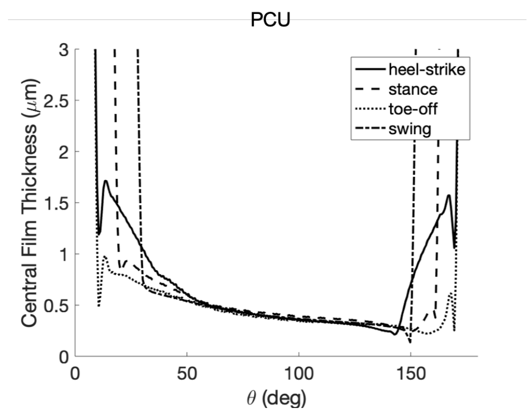

Figure 10: The film thickness along a central transect in the entraining direction for PCU shows a large difference between the leading a lagging film thickness and a minimum thickness at the leading edge between 0.13 and 0.24 μm ($\eta = 0.002$ $Pa \cdot s$, E = 24 MPa, radius = 17 mm).

Similar to the steady state solution, the transient solution predicts a lower fluid pressure in the PCU couple than the UHMWPE couple for all time points in the gait cycle (Figure 12). Both profiles of maximum pressure follow the same profile as the applied pressure of the gait cycle. The pressure for the PCU couple ranges from 1 to 6 MPa and the pressure for the UHMWPE couple ranges from 3 to 12 MPa.

In contrast to the results of the steady state solution, the minimum film

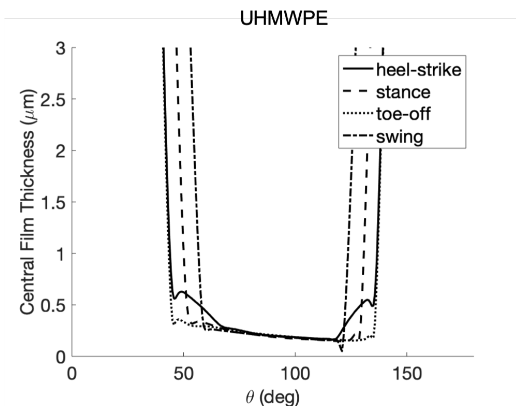

Figure 11: The film thickness along a central transect in the entraining direction for UHMWPE shows more consistent film thickness across the contact area with less difference between the leading and lagging edge and an overall lower minimum thickness than PCU of 0.05 to 0.16 μm ($\eta = 0.002\ Pa \cdot s$, E = 1000 MPa, radius = 17 mm).

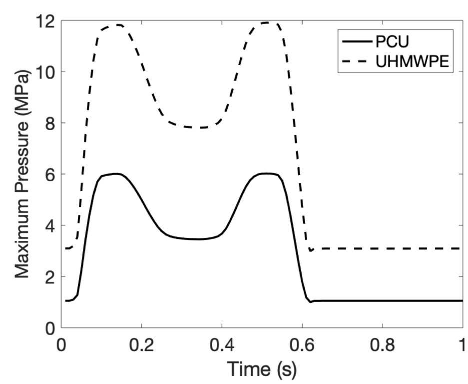

Figure 12: The maximum fluid pressure of PCU was consistently lower than that of UHMWPE. The pressure profiles of both materials reflected the pattern of the applied load ($\eta = 0.002\ Pa \cdot s$, $E_{UHMWPE} = 1000$ MPa, $E_{PCU} = 24$ MPa, radius = 17 mm).

thickness for the transient solution does not occur along the central axis of flexion-extension motion. This asymmetry reflects the contribution of the 3D rotations. As seen in Figures 13 and 14, the maximum pressure is symmetric and centered in the cup, but the minimum film thickness occurs in the anterior/lateral (upper right) region of the acetabular cup. This film thickness distribution varies throughout the gait cycle, but follows this trend asymmetric film thickness distribution.

Again, in contrast to the steady state solution, the minimum film thickness for the transient solution is lower for PCU than for UHMWPE. For both couples, the central film thickness remains relatively stable throughout the gait cycle and, like the steady state solution, is lower for UHMPWE than for PCU. However, the minimum film thickness is, on average, lower for PCU than that of UHMWPE and has a greater variability during the gait cycle (Figure 15, Table 5).

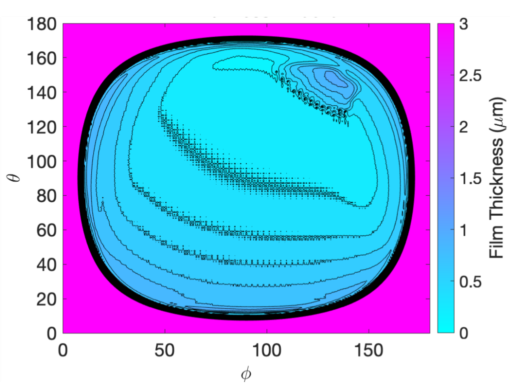

Figure 13: The asymmetry of the PCU film thickness distribution at toe-off demonstrates that the minimum film thickness is not correlated to the central film thickness and does not necessarily occur at the primary axis of flexion extension motion ($\eta = 0.002\ Pa \cdot s$).

Over the gait cycle, the film thickness of both materials does not follow a clear relationship to the applied load. For example, the minimum film

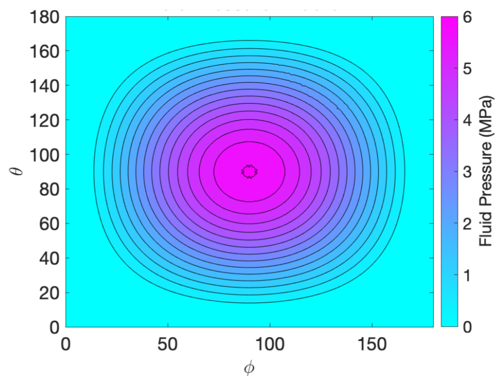

Figure 14: In contrast to the asymmetry of the PCU film thickness distribution, the PCU pressure distribution remained largely symmetric and centered throughout the gait cycle ($\eta = 0.002\ Pa \cdot s$).

thicknesses for both PCU and UHMPWE do not correspond to the times of maximum load. Conversely, the minimum film thickness is relatively high for both PCU and UHMWPE at heel-strike and toe-off (approximately 0.13 and 0.51s respectively) (Figure 15, center). For PCU, the central film thickness does trend with the maximum loads with dips in central film thickness when load is highest (Figure 15, bottom). UHMWPE follows the opposite trend. The central film thickness of UHMWPE has local maximums at heel-strike and toe-off (Figure 15, bottom).

In addition to having a lower minimum film thickness, the PCU couples also have a much greater contact area compared to UHMPWE (Figure 16). At the critical timepoints in the gait cycle, heel-strike, stance, toe-off, and swing, the contact area in the PCU couple ranges from 54 - 69% of the total area of the acetabular cup while the contact area in the UHMWPE cup ranges from 13 - 24 %. Additionally, the area where the film thickness is less

Table 4: Average and range of the central and minimum film thicknesses of PCU and UHMWPE throughout the gait cycle ($\eta = 0.002\ Pa \cdot s$, $E_{UHMWPE} = 1000$ MPa, $E_{PCU} = 24 MPa$, radius = 17 mm).

Material	Minimum Film Thickness (μm)		Central Film Thickness (μm)	
	Average	Range	Average	Range
UHMWPE	0.091	0.038 - 0.157	0.197	0.189 - 0.208
PCU	0.054	0 - 0.229	0.397	0.383 - 0.417

than 0.5 μm is, in the PCU couple, between 25 - 36 % of the total area of the acetabular cup, compared to 10 - 21 % in the UHMWPE couple.

The lubrication regimes are calculated as the ratio of the film thickness to the average surface roughness of the material couple (Equation 9). The surface roughness of UHMWPE is reported to be between 0.1 - 2.5 μm Mattei et al. (2011); Wang and Jin (2006). The surface roughness of PCU is reported to be between 0.03 and 0.78 μm Elsner et al. (2011).

Table 5: The average and range of the lubrication regimes (λ) of PCU and UHMWPE throughout the gait cycle are presented as calculated as a ratio of the minimum (h_{min}) or central (h_c) film thickness and an assumed surface roughness of 0.5 μm for both materials ($\lambda = \frac{h}{R_a}$).

Material	Lubrication Regime (λ)			
	h_{min}/R_a		h_c/R_a	
	Average	Range	Average	Range
UHMWPE	0.18	0.08 - 0.31	0.39	0.38 - 0.42
PCU	0.11	0 - 0.46	0.79	0.77 - 0.83

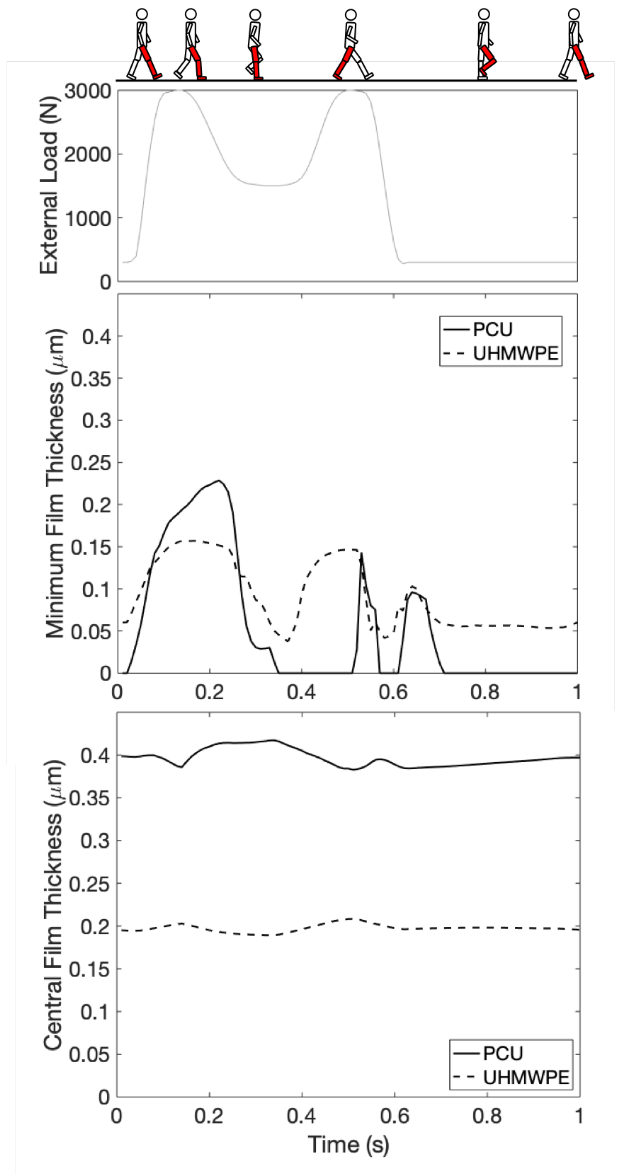

Figure 15: The minimum film thickness of PCU was, on average, lower than that of UHMWPE. In contrast, the central film thickness of PCU was higher than that of UHMWPE. Overall, there were mixed correlations between the applied external load and the film thicknesses in PCU and UHMWPE ($\eta = 0.002\ Pa \cdot s$, $E_{UHMWPE} = 1000$ MPa, $E_{PCU} = 24$ MPa, radius = 17 mm).

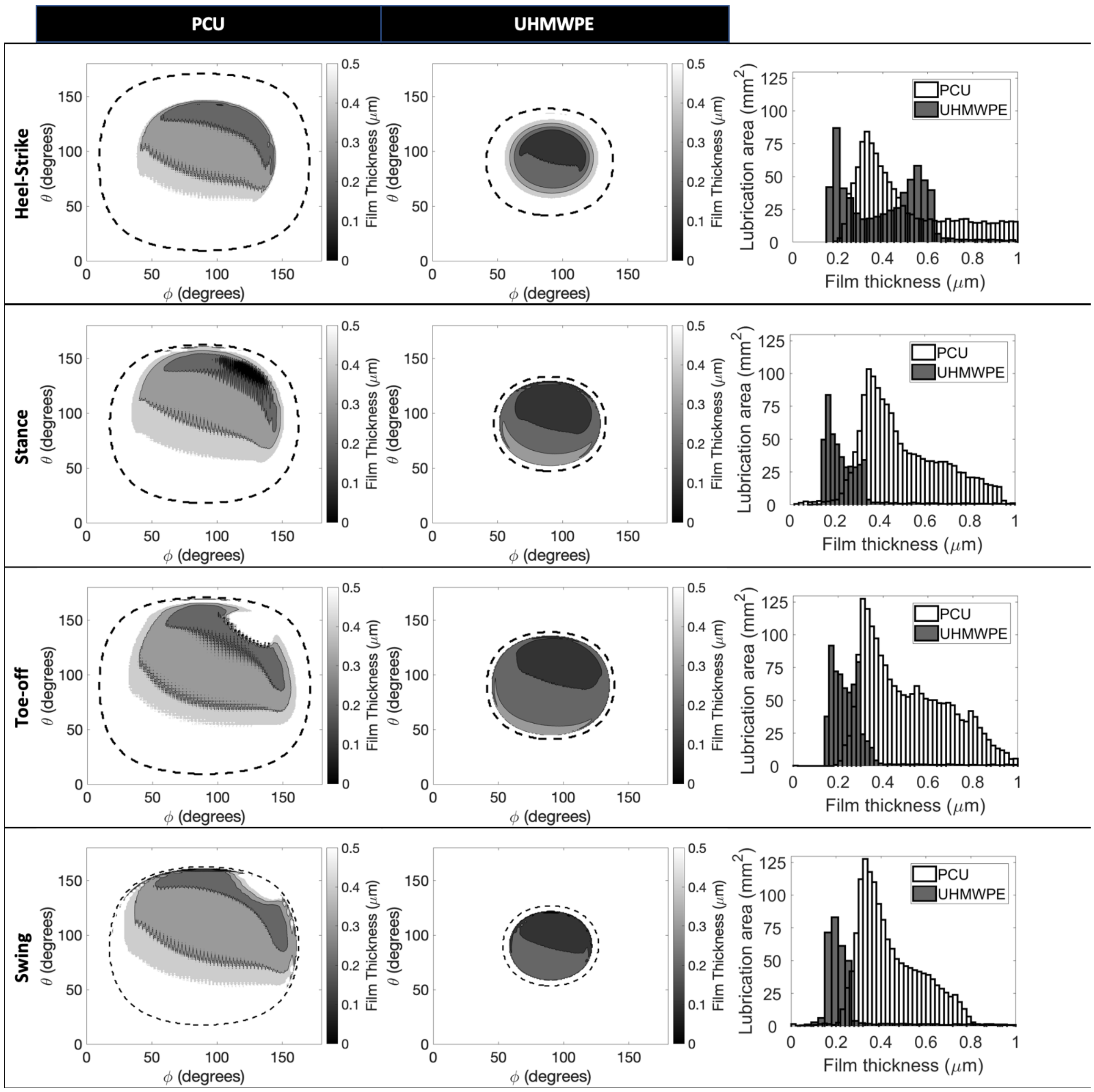

Figure 16: The total contact area (outlined with dotted line) is shown for PCU (left) and UHMWPE (center) at different stages of the gait cycle (from top to bottom: heel-strike, stance, toe-off, and swing). A comparison of the approximate area of the cup with a film thickness less than 1 μm for PCU and UHMWPE couples is shown on the right ($\eta = 0.002$ $Pa \cdot s$, $E_{UHMWPE} = 1000$ MPa, $E_{PCU} = 24$ MPa, radius = 17 mm).

4. Discussion and Conclusions

In this study, we present a 3D-transient EHL model to compare the impact of acetabular cup stiffness on the lubricant film thickness as an indicator of wear potential. Our model aligns with previous studies showing increased central film thickness in more compliant bearing surfaces. However, the 3D-transient model offers a more complex comparison, revealing an asymmetric distribution of minimum film thicknesses outside of the major axis of rotation and larger cyclic variations for the more compliant bearing couples.

Our results offer insights into the complex interactions that could contribute to limiting the wear performance of compliant bearing couples compared to the initial predictions of early EHL models that assumed 1D rotation and steady state conditions. Early models predicted full fluid film lubrication that would suggest large improvements in wear performance over current UHMWPE couples, but experimental wear studies showed mixed results, rather than an overwhelming improvement.

Compared to early steady-state models, our 3D-transient model reveals that, under 3D rotation, the minimum film thickness can occur off the main axis motion. The comparison of the central film thickness or average film thickness does not capture the differences between the distributions. The central film thickness of PCU was higher than that of UHMWPE for the entire gait cycle, However, the minimum film thickness for PCU was lower than that of UHMPWE for much of the gait cycle. Throughout the gait cycle, the PCU couple had larger variations in minimum film thickness, though not as much is central film thickness. Additionally, the contact area for PCU remained over 50% of the total cup area compared to less than 25% for the UHMWPE couple.

Previous studies suggested that the film thicknesses found in compliant, PCU, bearing couples would move towards a full fluid film lubrication regime Wang et al. (2004); Dowson et al. (1991). It has consistently been reported that UHMWPE operates in a mixed-lubrication regime with partial contact and partial lubrication and a higher potential for wear Jalali-Vahid et al. (2000, 2001); Jalali-Vahid and Jin (2002); Mattei et al. (2011); Lu et al. (2018).

This study predicts the boundary or mixed lubrication regimes for both PCU and UHMWPE couples, except in the case of PCU having a very low surface roughness ($\sim$0.03 μm). To approach full fluid lubrication regimes, the central film thickness of PCU would need to be several times higher than reported here ($\sim$0.4 μm). Additionally, the area covered by a given lubrication regime will have a significant influence on the potential wear. In Figure 14, the histograms show that in general, UHMWPE has a distribution of film thicknesses that is lower than that of PCU. However, the number of UHMWPE elements with that lower film thickness is much lower than the number of PCU elements at a slightly higher film thickness. All other things equal, it could be argued that the lower amount of contact in the PCU couple due to the higher film thickness is negated by the larger contact area.

However, the wear situation is dependent on many other contributing factors. The higher contact area also reduces the pressure, another important variable for wear. Additionally, the true surface roughness of the PCU vs. UHMPWE bearing surfaces are dependent on many processing variables. Finally, the wear potential of PCU and UHMWPE depends on the adhesive strength of the material couples. Each of these factors could alter the relative contribution of film thickness to wear potential.

The results of this study show that reducing the stiffness of the bearing material can increase the average film thickness, but in doing so also leads to localized areas with very low film thickness and increases the total area subject to mixed lubrication regimes.

One central assumption of this study is that PCU is a linear elastic material when PCU is indeed a non-linear and viscoelastic material Beckmann et al. (2018); Ghaill and Little (2008). A different material model would have significant impact on the calculated deformation. Viscoelastic material properties have been incorporated into EHL models Lu et al. (2018); Putignano and Dini (2017) and have shown that there is a slight increase in minimum film thickness. PCU, as a more compliant material with larger deformations, is likely that the impact of viscoelasticity will be greater than for that of UHMWPE and therefore is more important for the relevance of the model. Future work will aim to incorporate the nonlinear and viscoelastic properties of PCU into the current 3D-transient EHL model. Additionally, this study only presents the influence of different material stiffnesses under an equivalent geometry. Typical UHMWPE implant designs have a smaller radius, while the PCU acetabular cups are designed to be larger up to 25 mm in radius.

The objective of this study was to use a 3D-transient EHL model to investigate the impact of using a more compliant PCU acetabular cup, compared to a UHMWPE cup, in hip implants. In line with previous studies, we found that the average fluid film thickness in the PCU cup was higher than that of the UHMWPE cup. However, as a result of 3D rotations, we found that, for the majority of the gait cycle, the minimum film thickness of the PCU couple was lower than that of the UHMWPE couple. The film thickness distribution in the PCU couple was highly asymmetric and and minimum film thickness did not occur along the central axis of flexion-extension as would be assumed by models with only 1D rotation and loading. Our model provides insight into a more complex interaction between material stiffness and film thickness that can give insight into wear potential.

5. Acknowledgements

This work was supported by a Whitaker International Program Fellowship, the Ian Finnie Fellowship, and Shanghai Orthotek Lab Academic Funding.

6. References

Atwood, S. A., Citters, D. W. V., Patten, E. W., Furmanski, J., Ries, M. D., Pruitt, L. A., 2011. Tradeoffs amongst fatigue , wear , and oxidation resistance of cross-linked ultra-high molecular weight polyethylene. Journal of the Mechanical Behavior of Biomedical Materials 4 (7), 1033–1045.

Auger, D., Dowson, D., Fisher, J., 1995. Cushion form bearing for total knee joint replacement part 1: design, friction and lubrication. Proc Insta Mech Engrs 29, 73–81.

Beckmann, A., Heider, Y., Stoffel, M., Markert, B., 2018. Assessment of the viscoelastic mechancial properties of polycarbonate urethane for medical devices. Journal of the Mechanical Behavior of Biomedical Materials 82, 1–8.

Cadossi, M., Chiarello, E., Savarino, L., Tedesco, G., Baldini, N., Faldini, C., Giannini, S., 2013. A comparison of hemiarthroplasty with a novel polycarbonate-urethane acetabular component for displaced intracapsular fractures of the femoral neck. Bone and Joint Journal 95 (B), 509–515.

Dowson, D., Fischer, J., Jin, Z., Auger, D., Jobbins, B., 1991. Design considerations for cushino form bearing in artificial hip joints. Journal of Engineering in Medicine 205, 59–68.

Dowson, D., Jin, Z.-M., 1986. Micro-elastohydrodynamic lubrication of synovial joints. Engineering in medicine 15 (2), 63–65.

Elsner, J. J., Mezape, Y., Hakshur, K., Shemesh, M., Linder-Ganz, E., Shterling, A., Eliaz, N., 2010. Wear rate evaluation of a novel polycarbonate-urethane cushion form bearing for artificial hip joints. Acta Biomaterialia 6 (12), 4698–4707.

Elsner, J. J., Shemesh, M., Mezape, Y., Levenshtein, M., Hakshur, K., Shterling, A., Linder-Ganz, E., Eliaz, N., 2011. Long-term evaluation of a compliant cushion form acetabular bearing for hip joint replacement: A 20 million cycles wear simulation. Journal of Orthopaedic Research 29 (12), 1859–1866.

Flannery, M., Jones, E., Birkinshaw, C., 2010. Compliant layer knee bearings. Part II: Preliminary wear assessment. Wear 269 (5-6), 331–338.

Ford, A. C., Gramling, H., Li, S. C., Sov, J. V., Srinivasan, A., Pruitt, L. A., mar 2018. Micromechanisms of fatigue crack growth in polycarbonate polyurethane: time dependent and hydration effects. Journal of the Mechanical Behavior of Biomedical Materials 79, 324–331.

Gao, L., Hua, Z., Hewson, R., jul 2018. Can a “pre-worn” bearing surface geometry reduce the wear of metal-on-metal hip replacements? – a numerical wear simulation study. Wear 406-407, 13–21.

Gao, L., Wang, F., Yang, P., Jin, Z., jul 2009. Effect of 3d physiological loading and motion on elastohydrodynamic lubrication of metal-on-metal total hip replacements. Medical Engineering & Physics 31 (6), 720–729.

Ghaill, N. N. A., Little, E. G., may 2008. Determination of the mechanical properties of bionate 80a and bionate 75d for the stress analysis of cushion form bearings. Proceedings of the Institution of Mechanical Engineers, Part H: Journal of Engineering in Medicine 222 (5), 683–694.

Giannini, S., Chiarello, E., Cadossi, M., Luciani, D., Tedesco, G., 2011.

Prosthetic surgery in fragility ostopathy. Aging Clinical and Experimental Reserach 23 (2), 40–42.

Goodman, S. B., Ma, T., Chiu, R., Ramachandran, R., Smith, R. L., 2006. Effects of orthopaedic wear particles on osteoprogenitor cells. Biomaterials 27 (36), 6096 – 6101.

Ianuzzi, A., Kurtz, S. M., Kane, W., Shah, P., Siskey, R., van Ooij, A., Bindal, R., Ross, R., Lanman, T., Büttner-Janz, K., Isaza, J., 2010. In vivo deformation, surface damage, and biostability of retrieved Dynesys systems. Spine 35 (23), E1310–E1316.

Jacobs, J. J., Hallab, N. J., Urban, R. M., Wimmer, M. A., 2006. Wear particles. JBJS 88, 99–102.

Jalali-Vahid, D., Jagatia, M., Jin, Z., Dowson, D., 2000. Elastohydrodynamic lubrication analysis of uhmwpe and hip joint replacements. Thinning Films and Tribological Interfaces, 329–339.

Jalali-Vahid, D., Jagatia, M., Jin, Z., Dowson, D., 2001. Prediction of lubricating film thickness in uhmwpe hip joint replacements. Journal of Biomechanics 34, 261–266.

Jalali-Vahid, D., Jin, Z., 2002. Transient elastohydrodynamic lubrication analysis of and ultra-high molecular weight polyethylene hip joint and replacements. Proc. Instn Mech Engrs Part C: Journal of Mechanical Engineering Science 216, 409–420.

Jalali-Vahid, D., Jin, Z., Dowson, D., 2003. Elastohydrodynamiclubrication analysis of hip implants with ultra high molecular weight polyethylene cups under transient conditions. Proc Instn Mech Engrs 217 (C).

Jin, Z., Dowson, D., Fisher, J., Rimmer, D., Wilkinson, R., Jobbins, B., 1994. Measurement of lubricating film thickness in low elastic modulus lined bearings, with particular reference to models of cushion form bearings for total joint replacements: Part 1: steady state entraining motion. Proceedings of the Institution of Mechanical Engineers, Part J: Journal of Engineering Tribology 208 (3), 207–212.

Jin, Z. M., Dowson, D., may 2005. Elastohydrodynamic lubrication in biological systems. Proceedings of the Institution of Mechanical Engineers, Part J: Journal of Engineering Tribology 219 (5), 367–380.

Jin, Z. M., Dowson, D., Fisher, J., 1993. Wear and friction of medical grade polyurethane sliding on smooth metal counterfaces. Wear 162-164 (PART A), 627–630.

Kanca, Y., 2017. Tribological testing of potential hemiarthoplasty materials using a custom-designed multi-directional reciprocating rig. Ph.D. thesis, Imperial College London.

Kanca, Y., Milner, P., Dini, D., Amis, A. A., jun 2018. Tribological evaluation of biomedical polycarbonate urethanes against articular cartilage. Journal of the Mechanical Behavior of Biomedical Materials 82, 394–402.

Kurtz, S. M., 2015. UHMWPE Biomaterials Handbook: Ultra High Molecular Weight Polyethylene in Total Joint Replacement and Medical Devices, 3rd Edition. Elsevier.

Kurtz, S. M., Lau, E., Ong, K., Zhao, K., Kelly, M., Bozic, K. J., 2009. Future young patient demand for primary and revision joint replacement: National projections from 2010 to 2030. Clinical Orthopaedics and Related Research 467 (10), 2606–2612.

Kurtz, S. M., Pruitt, L., Jewett, C. W., Crawford, R. P., Crane, D. J., Edidin, A. A., 1998. The yielding, plastic flow, and fracture behavior of ultra-high molecular weight polyethylene used in total joint replacements. Biomaterials 19 (21), 1989–2003.

Lu, X., Meng, Q., Wang, J., Jin, Z., dec 2018. Transient viscoelastic lubrication analyses of UHMWPE hip replacements. Tribology International 128, 271–278.

Malito, L. G., Arevalo, S., Kozak, A., Spiegelberg, S., Bellare, A., Pruitt, L., 2018. Material properties of ultra-high molecular weight polyethylene: Comparison of tension, compression, nanomechanics and microstructure across clinical formulations. Journal of the mechanical behavior of biomedical materials 83, 9–19.

Mattei, L., Puccio, F. D., Piccigallo, B., Ciulli, E., 2011. Lubrication and wear modeling of artificial hip joints: A review. Tribology International 44, 532–549.

Moroni, A., Nocco, E., Hoque, M., Diremigio, E., Buffoli, D., Cantù, F., Catalani, S., Apostoli, P., aug 2011. Cushion bearings versus large diameter head metal-on-metal bearings in total hip arthroplasty: a short-term metal ion study. Archives of Orthopaedic and Trauma Surgery 132 (1), 123–129.

Putignano, C., Dini, D., 2017. Soft matter lubrication: does solid viscoelasticity matter? ACS applied materials & interfaces 9 (48), 42287–42295.

Scholes, S., Unsworth, A., Jones, E., 2007. Polyurethane unicondylar knee prostheses: simulator wear tests and lubrication studies. Physics in Medicine and Biology 52, 197–212.

Scholes, S. C., Burgess, I. C., Marsden, H. R., Unsworth, A., Jones, E., Smith, N., may 2006. Compliant layer acetabular cups: Friction testing of a range of materials and designs for a new generation of prosthesis that mimics the natural joint. Proceedings of the Institution of Mechanical Engineers, Part H: Journal of Engineering in Medicine 220 (5), 583–596.

Siebert, W. E., Mai, S., Kurtz, S., 2008. Retrieval analysis of a polycarbonate-urethane acetabular cup: a case report. Journal of long-term effects of medical implants 18 (1), 69–74.

Smith, R. A., Hallab, N. J., 2009. In vitro macrophage response to polyethylene and polycarbonate-urethane particles. Journal of Biomedical Materials Research - Part A 93 (1), 347–355.

Sonntag, R., Reinders, J., Kretzer, J. P., 2012. What's next? Alternative materials for articulation in total joint replacement. Acta Biomaterialia 8 (7), 2434–2441.

St. John, K., Gupta, M., 2012. Evaluation of the wear performance of a polycarbonate-urethane acetabular component in a hip joint simulator and comparison with UHMWPE and cross-linked UHMWPE. Journal of Biomaterials Applications 27 (1), 55–65.

Wang, F., Jin, Z., 2006. Lubrication modeling of artificial hip joints. IUTAM Symposium on Elastohydrodynamics and Microelastohydrodynamics, 385–396.

Wang, F., Liu, F., Jin, Z., 2004. A general elastohydrodynamic lubrication analysis of and artificial hip joints employing a compliant layered and socket under steady state rotation. Proc. Instn Mech Engrs Part H: Jounal of Engineering in Medicine 218, 283–291.

Willert, H., Bertram, H., Buchhorn, G., September 1990. Osteolysis in alloarthroplasty of the hip. the role of ultra-high molecular weight polyethylene wear particles. Clinical Orthopaedics and Related Research (258), 95107.

Wippermann, B., Kurtz, S., Hallab, N., Treharne, R., 2008. Explantation and analysis of the first retrieved human acetabular cup made of polycarbonate urethane: a case report. Journal of long-term effects of medical implants 18 (1), 75–83.